Hydrogen production from ammonia decomposition using Co/γ-Al2O3 catalysts – Insights into the effect of synthetic method

Bell, T. E.; Ménard, H.; González Carballo, J. M.; Tooze, R.; Torrente-Murciano, L.

Published in:
International Journal of Hydrogen Energy

DOI:
10.1016/j.ijhydene.2020.07.090

Publication date:
2020

Hydrogen production from ammonia decomposition using Co/γ-Al_2O_3 catalysts – insights into the effect of synthetic method

T. E. Bell,[1] H. Ménard,[2] J.-M. González Carballo,[3] R. Tooze[3] and L. Torrente-Murciano[1,*]

[1] *Department of Chemical Engineering and Biotechnology, University of Cambridge, West Cambridge Site, Philippa Fawcett Drive, Cambridge, CB3 0AS*

[2] *Leverhulme Research Centre for Forensic Science, University of Dundee, Dundee, DD1 4HN*

[3] *Drochaid Research Services, Purdie Building, North Haugh, St Andrews, Fife, KY16 9ST*

Abstract

Chemical hydrogen storage in molecules such as ammonia (> 17 wt% H_2) have the unique potential to overcome the current storage and transport limitations of the H_2 economy. However, sustainable on-demand production of hydrogen via ammonia decomposition, requires the development of novel transition metal-based catalysts beyond the current use of highly active but expensive ruthenium to ensure economic feasibility. In this paper, we provide fundamental understanding of the effects of a range of synthetic methods of Co/γ-Al_2O_3 catalysts on the resulting ammonia decomposition activity. The main activity determining factors are collectively the reducibility of the cobalt species and their particle size. This systematic work demonstrates that decreasing the cobalt particle size enhances the ammonia decomposition catalytic activity. However, a careful balance is required between a strong metal-support interaction leading to small particle sizes (promoted by precipitation methods) and the formation of inactive cobalt aluminate species (encouraged by adsorption methods). In addition, impurities such as boron and chloride remaining from particular synthetic methods were found to have detrimental effects on the activity.

[*] Corresponding author: Laura Torrente-Murciano, Phone: +441223 768664, Email: lt416@cam.ac.uk

Keywords:

cobalt, ammonia decomposition, alumina, hydrogen, synthesis method, heterogeneous catalysis.

Introduction

Hydrogen has been identified as a clean, alternative energy vector that could one day replace fossil fuels for portable applications.[1] The uptake of hydrogen-dependent technologies is currently limited by difficulties to economically store hydrogen with a sufficiently high density. In addition, public acceptance is low due to safety concerns regarding its physical storage and transportation.[2] Alternatively, hydrogen can be chemically stored in molecules such as methanol, methane, ammonia and its derivatives (e.g. NH_3BH_3), metal amine salts (e.g. $Mg(NH_3)_6Cl_2$ or $Ca(NH_3)_8Cl_2$) and metal hydrides (e.g. $LaNi_5H_6$ or $NaAlH_4$).[3,4]

Out of these compounds, ammonia is an attractive carbon-free option[5] owing to its high 17.6 wt.% hydrogen content, exceeding the 9 wt% target set by US Department of Energy in 2015. It also presents a narrow flammability range in air (16 to 25 vol%) compared to H_2 (4 to 75 vol%) and low pressure liquefaction (8 bar). The extensive use of ammonia in the fertiliser industry means that there are existing transportation and distribution networks, and established safety protocols to support the current large scale annual production (> 100 million tonnes).[3,6–9] The toxicity of ammonia may be concerning but the strong smell is practical for identifying leaks. Alternatively, metal amines can be used to safely store ammonia as a solid.[4,8]

In order for the ammonia molecule to be a viable route for hydrogen storage, on-demand H_2 production via its decomposition needs to be carried out at temperatures aligned with the operating temperature of a proton exchange membrane fuel cell (PEMFC), below 150 °C. The design of catalysts capable of effectively operating under these conditions is inherently challenging due to the endothermic nature of the reaction. Furthermore, at low temperatures, nitrogen desorption is the rate limiting step and thus the catalyst can be poisoned by strongly bound N-adatoms.[10] However, metal active sites still need to interact with nitrogen strongly enough to bind ammonia molecules but not so

strongly that the nitrogen atom cannot be desorbed after the N-H bonds have been cleaved. As a result, the metal-N binding energy is often used as a key parameter for ammonia decomposition catalyst design.[11,12]

The most effective reported catalysts for low temperature ammonia decomposition are based on electronically promoted ruthenium as it possesses an optimum nitrogen binding energy.[2,13–15] However, the cost and scarcity of ruthenium is impractical for large scale use in catalysis.[16] Thus, active catalysts based on readily available, non-noble metals need to be developed for low temperature NH_3 decomposition.[16,17] Our recent review on the subject identified cobalt as a possible replacement, however, the limited existing studies show poor activity, especially at low temperatures.[18]

It is well known in the catalysis field that the choice of nanoparticle synthesis method is critical as it can result in the formation of distinct particle sizes and can modify the metal-support interaction, both of which have implications on catalytic activity.[19] We have demonstrated that the ammonia decomposition activity of cobalt-catalysts is greatly enhanced when using microporous carbons compared to mesoporous or non-porous carbons, suggesting the importance of cobalt particle size to catalyse this reaction.[20] However, to date there is no robust systematic study on the effect of the cobalt loading method on the catalyst properties with the resulting ammonia decomposition activity. Herein we show the implications of the cobalt loading method on γ-alumina (including variations on impregnation, adsorption and precipitation techniques) on the ammonia decomposition activity owing to changes in the particle size, reducibility and composition. This study provides unique design guidelines to accelerate the understanding and discovery of active cobalt-based catalysts for this application.

2. Experimental

2.1 Synthesis of support

γ-Al_2O_3 support was prepared by a hydrothermal method as described in our previous work.[21] To summarise briefly, aqueous solutions of NaOH and $Al(NO_3)_3 \cdot 9H_2O$ are added to a Teflon lined steel autoclave in a 3.91:1 reagent ratio molar ratio (pH 11.2). The sealed autoclave remains in an air-circulating oven for 20 hours at 200 °C. The resulting white γ-AlOOH precipitate is obtained by centrifugation and is dried overnight at 80 °C under vacuum. The ground γ-AlOOH powder is calcined at 500 °C for 3 hours (3 °C·min^{-1} rate) to yield γ-Al_2O_3. The final γ-Al_2O_3 product is washed with distilled water and dried overnight at 80 °C under vacuum.

2.2 Cobalt loading

Cobalt is loaded onto the 2D γ-Al_2O_3 support using different methods including impregnation, adsorption and precipitation. The cobalt precursor is cobalt (II) nitrate hexahydrate ($Co(NO_3)_2 \cdot (H_2O)_6$, *Sigma Aldrich* 99.999 wt%) and all catalysts are prepared with a loading of 7.7 wt.% Co (assuming all cobalt is loaded). After synthesis, the catalysts are dried at 80 °C overnight under vacuum and all the catalysts herein are calcined at 250 °C (5 hours, 1 °C·min^{-1}). Catalysts are reduced at 580 °C (20 NmL·min^{-1} pure H_2 for 45 minutes, 5 °C·min^{-1}) prior to characterisation (when indicated) and before catalytic testing. The nomenclature for the catalysts follows *X*Co/Al_2O_3 where X is the actual cobalt loading determined by elemental analysis.

The methods of cobalt loading are summarised below:

Impregnation: Both incipient wetness impregnation (*IWI*) and wet impregnation (*imp*) methods were used, which differ by the volume of aqueous cobalt solution used. In IWI, a cobalt solution with a volume equal to the pore volume of the support (1.6 mL·g^{-1}) is added dropwise over the support. By contrast, for wet impregnation the support is added to an excess volume of cobalt solution (100 mL), stirred and heated to 60 °C for three hours. The solvent is removed by rotary evaporation.

Adsorption: The support and an excess aqueous volume (100 mL) are stirred and heated to 60 °C for three hours. The catalyst is separated from the supernatant by centrifugation (4000 rpm, 3 minutes).

Precipitation: The same procedure as the adsorption method is carried out but with the addition of a basic precipitant to the mixture. Four different precipitants were used including NaOH (0.125 mol), a carbonate buffer obtained from *Omega* (50 mL containing 0.26 wt% Na_2CO_3, 0.21 wt% $Na(CO_3)_2$, 0.01 wt% bromthymol blue and 99.52 wt% H_2O), a borate buffer from *Fisher Chemicals* (50 mL containing 0.5 wt% NaOH, 0.5 wt% H_3BO_3, 0.5 wt% KCl and 98.5 wt% H_2O) and urea (0.083 mol).

2.3 Characterisation

Temperature programmed reduction (TPR) is carried out using a Micromeritics Autochem 2920 using 20 $mL \cdot min^{-1}$ of 5 vol% H_2 in argon flow from ambient temperature to 900 °C at a heating ramp rate of 5 $°C \cdot min^{-1}$. The outlet gas is analysed using a thermal conductivity detector and in some cases, a mass spectrometer is used simultaneously. Crystalline phase identification of the samples is carried out by powder X-ray diffraction (pXRD) analysis using a Siemens Kristalloflex diffractometer with Cu Kα radiation (1.54 Å), operated at 40 kV and 40 mA. Inductively coupled plasma optical emission spectroscopy (ICP-OES) is used for precise chemical composition determination. To analyse solids by ICP-OES, acid digestion of the sample is carried out using aqua regia (3:1 acid mixture of 36 vol% HCl and 70 vol% HNO_3) heated to 90 °C. The diluted solutions are analysed by a Perkin Elmer Optima 2100 DV spectrometer with argon as the torch gas and nitrogen for purging. The specimens are prepared for transmission electron microscopy (TEM) analyses by placing one drop of the sample suspended in ethanol onto a carbon-coated 300 mesh copper mesh grid (C300Cu, EMResolutions). High angle annular dark field scanning transmission electron microscopy (HAADF-STEM) is carried out on a TESCAN MIRA3 at 30kV accelerating voltage. X-ray photoelectron spectroscopy (XPS) analyses are carried out on a KRATOS Axis Ultra DLD instrument. Approximately 10 mg of sample is mounted as a loose powder in a molybdenum sample holder. The measurements are carried out using an achromatic Al kα source (15 kV, 10 mA). The position of aluminium (Al 2p) at 74.0 eV is used for spectral calibration.

2.4 Catalyst testing

For a typical ammonia decomposition reaction, 25 mg of catalyst is evenly dispersed in a packed bed with 450 mg of inert coarse silicon carbide (360 μm) diluent inside a U-shape quartz reactor preceded by 175 mg of fine silicon carbide (53 μm). The coarse silicon carbide avoids a high pressure drop and the fine silicon carbide ensures plug flow. The temperature of the packed bed is regulated by an external tubular furnace (*Carbolite*) and a type K thermocouple above the exit of the catalyst bed. Catalysts are pre-reduced in-situ at 580 °C for 45 minutes to ensure complete reduction under these conditions. After that, a mixture of NH_3 (2.5 $NmL \cdot min^{-1}$) and He (6 $NmL \cdot min^{-1}$) is continuously fed into the reactor giving a gas hourly space velocity (GHSV) of 6000 $mL_{NH3} \cdot g_{cat}^{-1} \cdot h^{-1}$. The outlet gas stream flows through a gas chromatograph (*Agilent 7820A*) equipped with a *Porapak Q* column, a thermal conductivity detector (TCD) and a 6-way value enabling automated sampling. Only hydrogen and nitrogen are detected as products. During the catalytic test, the temperature is increased from ambient up to 580 °C at a rate of 2.6 $°C \cdot min^{-1}$ for three consecutive heating and cooling runs. In all cases, the reported activity corresponds to the third heating run.

3. Results and discussion

A range of synthetic methods have been screened to produce cobalt nanoparticles supported 2D alumina in order to gain a fundamental understanding of the key parameters affecting the activity of cobalt nanoparticles for the release of hydrogen via ammonia decomposition. The methods used are incipient wetness impregnation (*IWI*), impregnation (*imp*), adsorption (*ads*), and precipitation with NaOH (*NaOH*), carbonate buffer (*carb*), borate buffer (*bor*) and urea (*urea*). The choice of the 2D alumina supports provides the same γ-Al_2O_3 surface chemistry and morphology (Figure S1) across all the materials.

Figure 1 shows the conversion versus temperature graph as well as the Arrhenius plot for each of the catalysts. Apparent rate of reaction and TOF values are calculated taking into consideration the actual

cobalt loading in each catalyst determined by ICP-OES. All the studied catalysts are active for the ammonia decomposition reaction at temperatures above 380°C, except the catalyst prepared by adsorption which shows activity only at temperatures above 470°C.

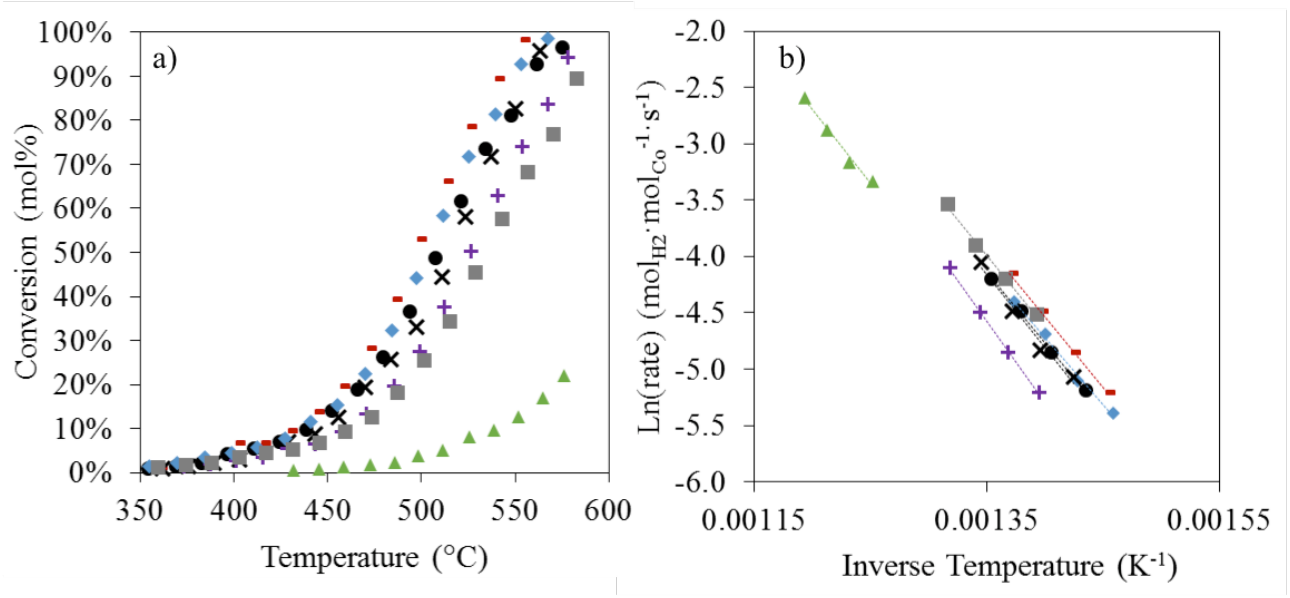

Figure 1. NH_3 decomposition catalytic data for *Co/Al_2O_3* catalysts synthesised by different methods a) activity as a function of temperature and b) Arrhenius plot. ● (*$7.7Co/Al_2O_3$-IWI*), ◆ (*$7.7Co/Al_2O_3$-imp*), ▲ (*$1.4Co/Al_2O_3$-ads*), X (*$6.8Co/Al_2O_3$-NaOH*), - (*$7.6Co/Al_2O_3$-carb*), + (*$7.3Co/Al_2O_3$-bor*), ■ (*$3.8Co/Al_2O_3$-urea*).

All the preparation methods used in this study use 7.7 wt.% nominal cobalt loading. This loading has been found to be optimal on ruthenium supported on carbon nanotubes as it maximises the concentration of B_5 active sites.[2] It is currently unknown in the literature what specific arrangement of cobalt atoms are responsible for catalysing N-H bond cleavage, not least the loading required to maximise the active cobalt clusters. As the focus of this work was to elucidate the effect of the synthetic method on the final ammonia decomposition activity, the same theoretical 7.7 wt% Co loading was used without further optimisation. However, the actual cobalt loading was found to vary with each method based on the quantification by ICP-OES, (Table 1). In order to compare the ammonia decomposition activity of the different methods, turn-over frequency values per amount of cobalt at a given temperature (500°C) were calculated as shown in Table 1. In this way, it is clear that the low activity observed for the *$1.4Co/Al_2O_3$-ads* catalyst is not solely due to its low cobalt loading.

Table 1. Synthesis parameters, properties and ammonia decomposition catalytic activity of calcined Co/Al_2O_3 catalysts synthesised by different methods.

Catalyst	Method	Initial pH [a]	Catalyst colour [b]	Impurities [c]	Content (wt%) [b, d]		TOF @ 500 °C [b] ($mol_{H2}·mol_{Co}^{-1}·h^{-1}$)	E_a [b] ($kJ·mol^{-1}$)
					Co	Na		
7.6Co/Al_2O_3-carb	Carbonate buffer precipitation	9.3	Dark green	C, Na	7.6	3.0	156.4	105.3
3.8Co/Al_2O_3-urea	Urea precipitation	5.9	Violet	C, Na, N	3.8	1.8	142.3	104.2
7.7Co/Al_2O_3-imp	Impregnation	n/a	Dark brown	C, Na	7.7	2.6	131.8	99.1
7.7Co/Al_2O_3-IWI	IWI	n/a	Black	C, Na	7.7	2.7	120.3	103.9
6.8Co/Al_2O_3-NaOH	NaOH precipitation	10.8	Dark green	C, Na	6.8	8.4	113.4	108.6
7.3Co/Al_2O_3-bor	Borate buffer precipitation	9.8	Dark green	C, Na, B, Cl, K	7.3	2.2	83.6	120.0
1.4Co/Al_2O_3-ads	Adsorption	6.5	Light khaki green	C, Na	1.4	1.5	62.6	120.7

[a] pH of the cobalt precursor solution in the presence of precipitant.
[b] Reduced at 580°C.
[c] Determined by XPS (in addition to Al, O and Co expected elements).
[d] Calculated from ICP-OES of the digested calcined solid.

The activity of the catalysts per amount of cobalt increases across the series in the order *1.4Co/Al_2O_3-ads < 7.3Co/Al_2O_3-bor < 6.8Co/Al_2O_3-NaOH < 7.7Co/Al_2O_3-IWI < 7.7Co/Al_2O_3-imp < 3.8Co/Al_2O_3-urea < 7.6Co/Al_2O_3-carb.* As shown in Figure 2, there is not a direct relationship between ammonia decomposition activity and cobalt loading for the catalysts prepared by different methods. It is interesting to note that while the activation energy values of the most active catalysts ranges between 100 and 108 kJ mol^{-1}, the catalysts prepared by borate buffer precipitation and adsorption have higher values of activation energy (~ 120 $kJ·mol^{-1}$), suggesting the presence of different active sites.

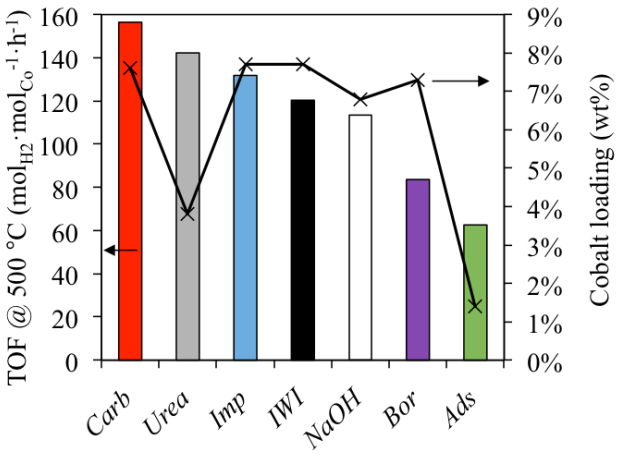

Figure 2: Ammonia decomposition turnover frequency values at 500 °C for the *Co/Al₂O₃* catalysts (reduced at 580 °C) synthesised by different methods and their actual cobalt loading.

The catalytic activity of nanoparticles is known to have a strong relationship with their size.[22] This activity-size relationship is particularly strong in the case of cobalt-catalysed NH_3 decomposition.[20] However, determination of the optimum catalytic size for this system is complex because other complimentary parameters such as metal-support interaction may also play a role in determining the activity.[23–25] In the case of *Co/Al₂O₃* catalysts, cobalt particle size determination by conventional imaging is not reliable due to the similarity in contrast between bulk alumina support and the cobalt. Indeed, Figure 3 shows representative bright and dark field micrographs of the *7.6Co/Al₂O₃-carb* catalyst where some of the dark spots on the bright field picture appear brighter in dark field (Figure 3b) but remain challenging to interpret at high magnification, leading to potential size distribution misinterpretations.

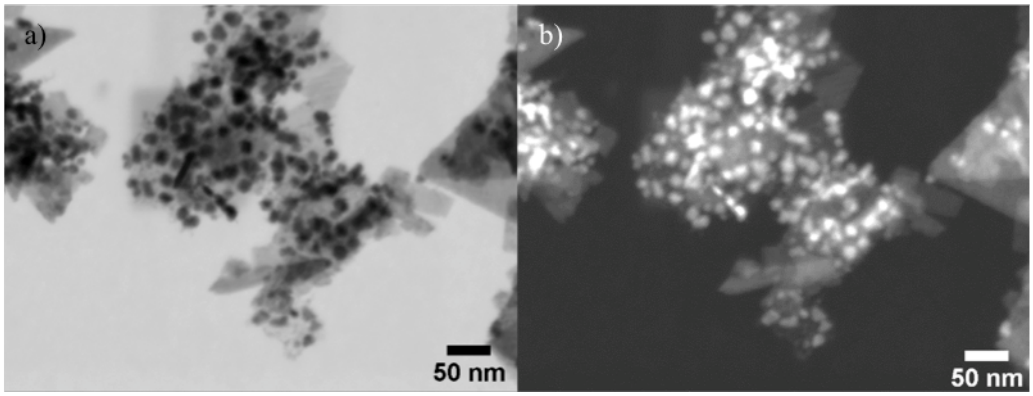

Figure 3. Representative (a) bright and (b) dark field SEM micrographs of *7.6Co/Al_2O_3-carb*.

As a result, powder X-ray diffraction (pXRD) was used to estimate the average cobalt crystallite size in the catalysts before and after reduction at 580 °C (Figure 4). The pXRD pattern of the alumina support shows diffraction peaks at 40°, 46° and 67°, assigned to γ-Al_2O_3 (JCPDS 10-0425). All the fresh calcined catalysts (Figure 4a) present diffraction peaks associated to the alumina support. Unfortunately, these diffraction peaks overlap with the major peaks associated to cobalt aluminate and CoO so these species cannot be identified separately. However, the diffraction peaks at ~ 37° and ~ 44° can be used to identify Co_3O_4 and cubic Co^0, respectively.[26–28] Well-defined Co_3O_4 peaks are visible in the *7.7Co/Al_2O_3-IWI* and *7.7Co/Al_2O_3-imp* catalysts, with associated average size of 10.5 and 14.5 nm, respectively (Table 2). The absence of Co_3O_4 diffraction peaks in the *1.4Co/Al_2O_3-ads* material may be due to its low metal loading. Co_3O_4 diffraction peaks are also absent for the catalysts produced by precipitation, suggesting that a calcination temperature above 250 °C may be needed to form crystalline Co_3O_4.[29] The pXRD patterns of *3.8Co/Al_2O_3-urea* and *7.7Co/Al_2O_3-IWI* (Figure 4) show an additional peak at ~ 28° due to the presence of $NaNO_3$ (JCPDS 36-1474)[30] in both the calcined and the reduced diffractograms. Calcination or reduction of catalysts at higher temperatures (above 580 °C reduction temperature) could have removed the presence of $NaNO_3$, however, this could have triggered agglomeration of the cobalt species, which is undesirable for this study.

Adsorption is normally a popular method for obtaining small particle sizes by promoting strong metal-support interactions,[31] however, depending on the surface chemistry of the support, low metal

loadings can be achieved like in this particular case with Co/γ-Al_2O_3. Indeed, the low loading arises from the fact that the acidic nature of the cobalt precursor decreases the pH of an aqueous cobalt nitrate solution mixed with γ-Al_2O_3 to pH 6.5, below the point of zero charge (PZC) for γ-Al_2O_3, which ranges from pH 7 to 10.[32] Thus, cobalt cation loading is electrostatically unfavourable, resulting in low cobalt loading. To overcome this limitation, a series of basic precipitants were used to raise the pH above the PZC to induce cobalt precipitation and facilitate higher cobalt loadings as shown in Table 1.

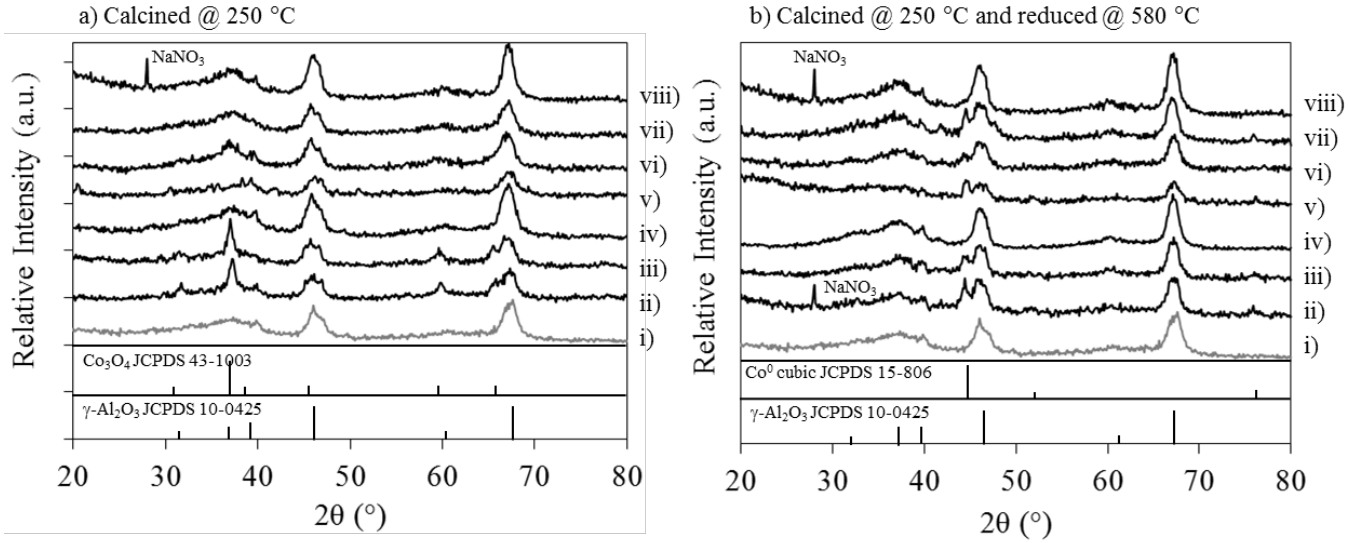

Figure 4. pXRD spectra of *Co/Al_2O_3* samples synthesised by different methods a) fresh calcined at 250°C and b) reduced at 580°C i) Al_2O_3 support (grey), ii) *7.7Co/Al_2O_3-IWI*, iii) *7.7Co/Al_2O_3-imp*, iv) *1.4Co/Al_2O_3-ads*, v) *6.8Co/Al_2O_3-NaOH*, vi) *7.6Co/Al_2O_3-carb*, vii) *7.3Co/ Al_2O_3-bor* and viii) *3.8Co/Al_2O_3-urea*. γ-Al_2O_3 JCPDS 10-0425, Co_3O_4 JCPDS 43-1003, Co^0 JCPDS 15-806, $NaNO_3$ JCPDS 36-1474.

After reduction at 580 °C, in addition to the pXRD peaks associated to the γ-Al_2O_3 support, Co^0 peaks are visible in the *7.7Co/Al_2O_3-IWI, 7.7Co/Al_2O_3-imp, 6.8Co/Al_2O_3-NaOH, 7.6Co/Al_2O_3-carb* and *7.3Co/Al_2O_3-bor* catalysts (Figure 4b).

The line broadening of the pXRD diffraction peaks for both calcined (250 °C) and reduced (580 °C) catalysts was used with the Scherrer equation to calculate the average crystallite size of Co_3O_4 and

Co^0 respectively (Table 2). The data shows that the ammonia decomposition catalytic activity of the different catalysts generally increases as the Co^0 crystallite size decreases. It is important to note that the reported Co^0 sizes might be overestimated due to the exposure of the catalysts to air prior to pXRD analysis as particles less than 4 nm are thermodynamically capable of re-oxidising and are below the detection capability of pXRD.[33] It is not possible to estimate the extent of oxidation by pXRD due to the overlap of the CoO diffraction peaks with those of the alumina support, however the trend of size increase should not be affected.

Table 2. Average cobalt particle sizes and Co^{2+} reduction temperatures of *Co/Al_2O_3* catalysts synthesised by different methods.

Catalyst	Average Co_3O_4 particle size [a] (nm)	Average Co^0 particle size [b, c] (nm)	Co^{2+} to Co^0 reduction temperature (°C)
7.6Co/Al_2O_3-carb	No peak	7.7	535.1, 588.6
3.8Co/Al_2O_3-urea	No peak	No peak	537.8
7.7Co/Al_2O_3-imp	14.5	9.3	405.0, 513.1
7.7Co/Al_2O_3-IWI	10.5	11.1	463.3
6.8Co/Al_2O_3-NaOH	No peak	14.8	494.0, 574.0
7.3Co/Al_2O_3-bor	No peak	17.0	549.5
1.4Co/Al_2O_3-ads	No peak	No peak	604.5

[a] Calculated using the FWHM of the Co_3O_4 at ~ 37° (JCPDS 43-1003) with the Scherrer equation.
[b] Calculated using the FWHM of the deconvoluted cubic Co peak at ~ 44° (JCPDS 15-806) with the Scherrer equation.
[c] Reduced at 580°C.

X-ray photoelectron spectroscopy (XPS) was used to identify the cobalt species formed by each of the synthesis methods. The shape of the multiplet XPS cobalt envelope enables identification of the cobalt oxidation state (Co^0, Co^{2+} and Co^{3+}), facilitated by the fittings of Biesinger *et al.*[34] for Co_3O_4, $Co(OH)_2$, CoO and Co^0. The XPS spectra of the calcined catalysts in Figure 5 confirms the surface

cobalt species to be Co_3O_4 in all the catalysts except *3.8Co/Al_2O_3-urea*, which is predominantly Co^{2+} with minor Co_3O_4. The confirmation of Co_3O_4 by XPS combined with the lack of Co_3O_4 pXRD diffraction peaks of *6.8Co/Al_2O_3-NaOH*, *7.6Co/Al_2O_3-carb* and *7.3Co/Al_2O_3-bor* catalysts, suggest that Co_3O_4 is poorly crystalline or amorphous in these catalysts. By contrast, for the catalysts obtained by the impregnation methods (*IWI* and *imp*), clear Co_3O_4 pXRD diffraction peaks were observed, indicative of crystalline Co_3O_4. Indeed, only the *7.7Co/Al_2O_3-IWI* and *7.7Co/Al_2O_3-imp* catalysts present a black/brown colour (Table 1), characteristic of Co_3O_4.[35] In the case of the *3.8Co/Al_2O_3-urea* catalyst, the envelope of the Co^{2+} set of XPS peaks (pink line in Figure 5g) has a similar shape as the fitted curves for CoO or $Co(OH)_2$ reported by Biesinger *et al.*[34], with the peak at 786 eV confirming Co^{2+} is the oxidation state. However, the binding energy values closely agree with the spectra of Yang *et al.*[36] for cobalt hydroxide carbonate ($Co_2CO_3(OH)_2$), suggesting this is the nature of the dominant Co^{2+} species, in agreement with the violet catalyst colour and the absence of Co_3O_4 pXRD diffraction peaks.

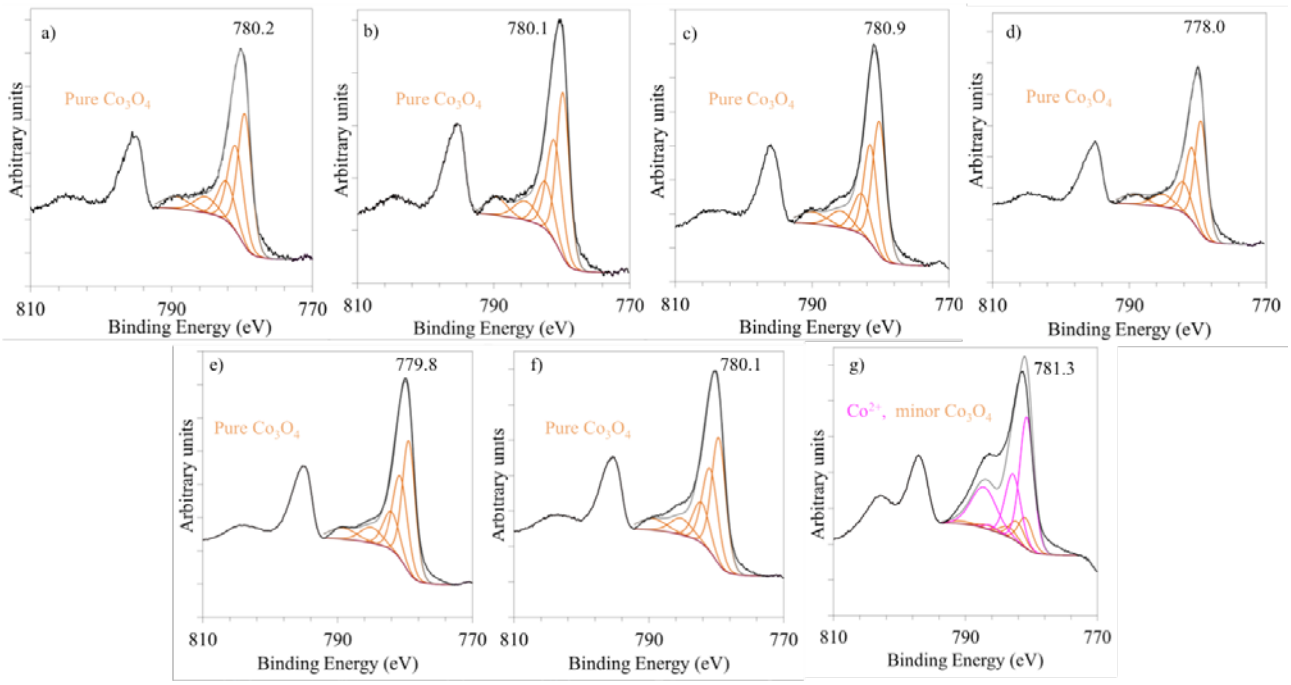

Figure 5. Co 2p XP spectra for the fresh calcined catalysts synthesised by different methods a) *7.7Co/Al_2O_3-IWI*, b) *7.7Co/Al_2O_3-imp*, c) *1.4Co/Al_2O_3-ads*, d) *6.8Co/Al_2O_3-NaOH*, e) *7.6Co/Al_2O_3-carb*, f) *7.3Co/Al_2O_3-bor* and g) *3.8Co/Al_2O_3-urea*. Black lines = raw data, orange lines are fitted to Co_3O_4 and pink lines are fitted to CoO.

Further information regarding the effects of the different synthetic methods on the resulting cobalt species as well as the metal-support interaction was obtained by analysis of temperature programmed reduction (TPR) profiles (Figure 6) and XPS analysis with *in situ* reduction (Figure 7). The TPR profiles of all the catalysts have been peak fitted and the different reduction steps have been assigned and colour-coded in Figure 6. Analysis of the outlet gases during TPR characterisation by mass spectrometry enables the distinction between reduction peaks and those due to the removal of impurities such as carbon and nitrates. The reduction profile of the γ-Al_2O_3 support is shown by the dashed black lines for reference, showing its negligible overall effect on the signal relative to the reduction of other species present in the catalyst. The dashed vertical purple line at 580 °C on the graphs represents the reduction temperature prior to ammonia decomposition catalytic testing.

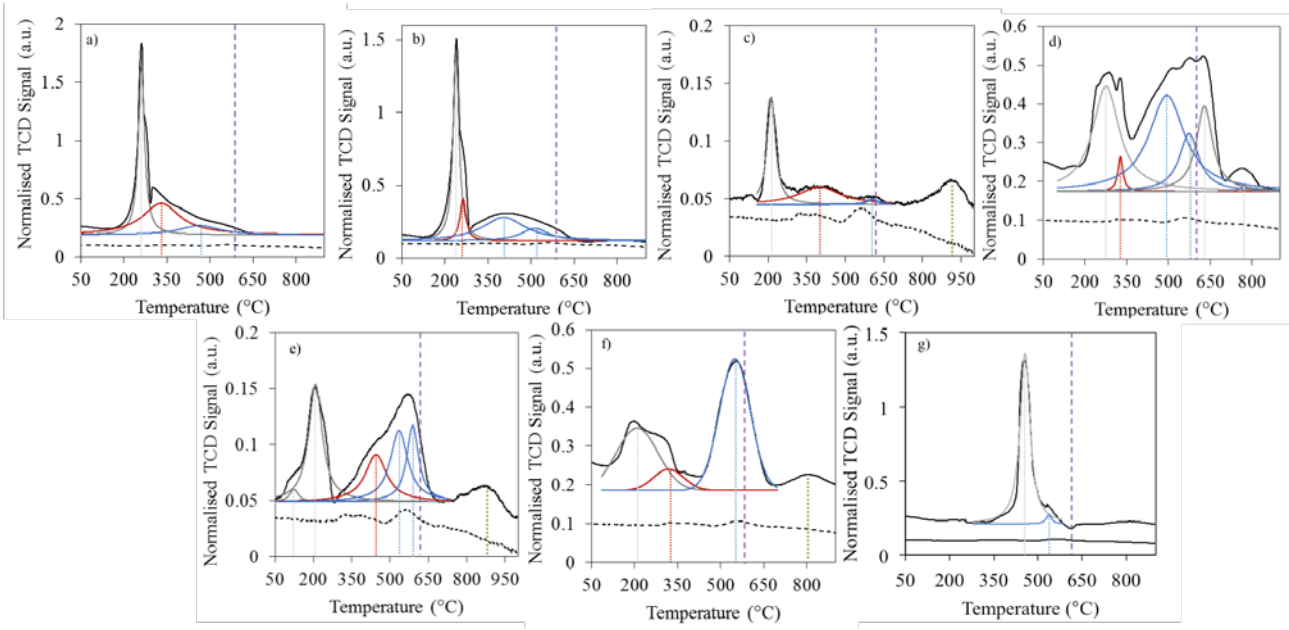

Figure 6. TPR profiles of the calcined *Co/Al_2O_3* catalysts synthesised by different methods. a) *$7.7Co/Al_2O_3$-IWI*, b) *$7.7Co/Al_2O_3$-imp*, c) *$1.4Co/Al_2O_3$-ads*, d) *$6.8Co/Al_2O_3$-NaOH*, e) *$7.6Co/Al_2O_3$-carb*, f) *$7.3Co/Al_2O_3$-bor* and g) *$3.8Co/Al_2O_3$-urea*. Normalised TCD signal = black line, alumina support TCD signal = black dashed line, chosen 580 °C reduction temperature = vertical purple dashed line. Fitted envelope peaks: Co^{3+} → Co^{2+} = burgundy line, Co^{2+} → Co^0 = blue line, $CoAl_2O_4$ → Co^0 = green curve and removal of impurities = grey line.

Cobalt reduction typically follows a two-step process from Co^{3+} to Co^{2+} to Co^{0}.[37] Additional processes identified by TPR include the reduction of irreducible cobalt aluminate species from 800 to 1000 °C and the removal of impurities such as carbon or nitrogen.[33,38] In all the catalysts, except for the *3.8Co/Al_2O_3-urea*, the TPR profile (Figure 6) shows a reduction peak associated to the first cobalt reduction step from Co^{3+} to Co^{2+} (burgundy line) which usually takes place from 260 to 450 °C.[26,33,39,40] The Co^{3+} reduction takes place towards the high temperature end of this range (444 °C) for the *7.6Co/Al_2O_3-carb* catalyst, suggesting a strong metal-support interaction, although the intensity of this peak is relatively low. It is likely that this high reduction temperature is directly associated to small particle size, in agreement with pXRD, leading to a high ammonia decomposition catalytic activity. In the case of the *3.8Co/Al_2O_3-urea* catalyst, the absence of a Co^{3+} reduction peak is in agreement with the XPS identification of $Co_2CO_3(OH)_2$ rather than the typical Co_3O_4 mixed oxide present in the other catalysts, as discussed earlier in this paragraph.

ICP-OES elemental analyses of the fresh calcined catalysts reveal the presence of impurities in the catalysts (Table 1), with residual carbon present in all the catalysts. Removal of this carbon during reduction was observed by TPR-MS of the *7.6Co/Al_2O_3-carb* catalyst at around 200 °C (Figure 6e), based on a mass spectrometry peak at m/z 16, indicative of CH_4 evolution. Similarly, the *3.8Co/Al_2O_3-urea* catalyst exhibits a high temperature methanation peak at 456.3 °C (Figure 6g) in agreement with a decrease in carbon content from 3.2 wt% to 0.4 wt% after reduction at 580 °C as determined by XPS composition data. Removal of residual nitrates by conversion to nitrogen at temperatures below 225 °C was observed for the catalysts synthesised by impregnation, adsorption and precipitation with a borate buffer, confirmed by a m/z 28 mass spectrometry peak.[28]

The second reduction step (Co^{2+} to Co^{0}) requires relatively high temperatures with Al_2O_3 supports as the Co-Al_2O_3 metal-support interaction is stronger than with common supports such as carbon materials and other metal oxides.[20,38] This strong interaction is evidenced by a broad, high

temperature Co^{2+} reduction peak in the range of 400 °C to 800 °C.[40,41] In several cases, such as *7.7Co/Al_2O_3-imp, 6.8Co/Al_2O_3-NaOH* and *7.6Co/Al_2O_3-carb* catalysts, this second reduction peak is fitted to two peaks, indicative of different metal-support interactions, potentially associated to a broad particle size distribution. In general, for a given system, a shift of the Co^{2+} to Co^0 reduction temperature towards higher values is related to both smaller particle sizes and/or stronger metal-support interaction.[38]

Taking into consideration that Co^0 is generally accepted as the active species for the ammonia decomposition reaction,[40] one can make a direct link between species reducibility and catalytic activity. For example, comparing the two catalysts synthesised by impregnation methods (*imp* and *IWI*), the former presents a higher activity and lower particle size than the latter which is reflected by similar shape TPR profiles shifted to slightly higher reduction temperatures in the case of the more active *imp* catalyst. This size-activity relationship also explains the high catalytic activity of the *7.6Co/Al_2O_3-carb* catalyst. Based on this correlation, similar high activities should be expected for the *6.8Co/Al_2O_3-NaOH* and *7.3Co/Al_2O_3-bor* catalysts however, in the first case the methanation peak observed around 630 °C in the TPR profile indicates residual carbon in the catalyst after reduction at 580 °C. The presence of carbon could be detrimental to activity as it may affect the accessibility of the active sites. In the case of the *7.3Co/Al_2O_3-bor*, ICP-OES analysis shows that the catalyst contains contaminants such as B and Cl, believed to be derived from the synthetic method (as the borate buffer precipitant is composed of 0.5 wt% of NaOH, H_3BO_3 and KCl). The presence of these contaminants may explain the lower activity of *7.3Co/Al_2O_3-bor* (Figure 1).[42,43] It is important to mention that all the catalysts contain sodium from the hydrothermal route used in the synthesis of the alumina support (Table 1), which is present despite catalyst washing. However, the presence of sodium is not believed to considerably affect the catalytic activity, as we have previously demonstrated that group 1 electron donating elements such as cesium do not alter the ammonia decomposition catalytic activity of cobalt-based catalysts.[20]

Another important parameter to consider is the reducibility degree of the cobalt species depending on the preparation method. XPS characterisation of the *in situ* reduced catalysts is shown in Figure 7, in which the catalysts generally show the Co^0 characteristic peaks with minor contributions from Co^{2+}. In the case of *7.7Co/Al_2O_3-IWI, 7.7Co/Al_2O_3-imp, 6.8Co/Al_2O_3-NaOH* and *7.6Co/Al_2O_3-carb*, the Co^{2+} contribution fits with the presence of CoO according to the peak fitting of Biesinger *et al.*[34]. However, the prevalence of larger Co^{2+} peaks after reduction in the *1.4Co/Al_2O_3-ads, 7.3Co/Al_2O_3-bor* and *3.8Co/Al_2O_3-urea* catalysts and their poor fitting to CoO suggests the presence of a different Co^{2+} species, such as $CoAl_2O_4$ or Co_2AlO_4 (cobalt aluminates). Indeed, the presence of cobalt aluminate species is confirmed in the TPR profiles of these catalysts by the presence of a high temperature reduction peak above 800 °C, assigned to the reduction of cobalt aluminates, $CoAl_2O_4$ to Co^0. The high reduction temperature gives rise to their description as "irreducible".[33,38]. Due to the low loading, the abundance of these cobalt aluminates is suggested by the catalyst colour in the case of *1.4Co/Al_2O_3-ads* as the catalyst remains pale blue (characteristic colour of cobalt aluminate) after reduction at 580 °C, however the catalyst is transformed to a black powder containing metallic cobalt after reduction at 1000 °C. The reduction peak centred at 770 °C in the TPR profile of *6.8Co/Al_2O_3-NaOH* catalyst (Figure 6d) is similar to that observed for unsupported cobalt nanoparticles precipitated by NaOH and therefore the peak is not believed to be due to $CoAl_2O_4$ reduction.

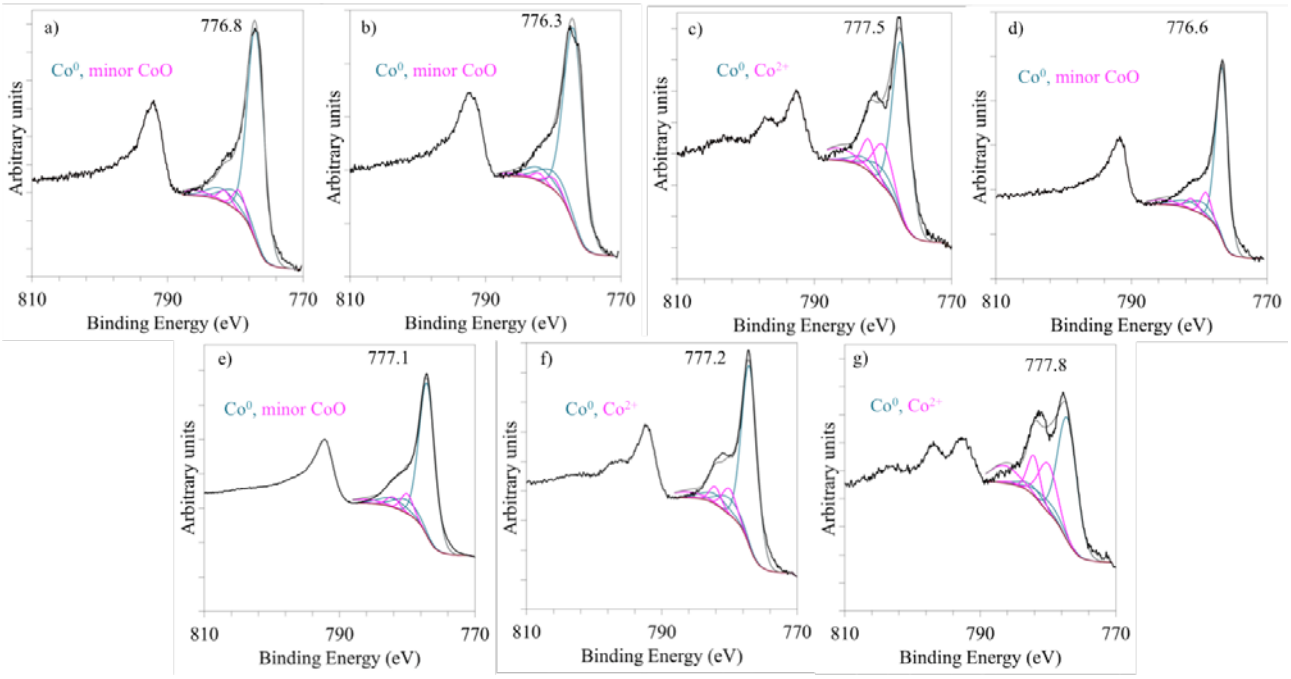

Figure 7. Co 2p XPS spectra for the in-situ reduced catalysts (580 °C) synthesised by different methods a) *7.7Co/Al_2O_3-IWI*, b) *7.7Co/Al_2O_3-imp*, c) *1.4Co/Al_2O_3-ads*, d) *6.8Co/Al_2O_3-NaOH*, e) *7.6Co/Al_2O_3-carb*, f) *7.3Co/Al_2O_3-bor* and g) *3.8Co/Al_2O_3-urea*. Black lines = raw data, pink lines are fitted to CoO and blue lines are fitted to Co^0.

According to XPS data, all the catalysts, independent of their synthetic method, contain unreduced species after reduction at 580 °C, in agreement with the TPR discussion above. The proportion of Co^0 after reduction is quantified by comparing the cumulative area under the Co^0 peaks relative to the total cobalt peaks area, as shown in Figure 8.

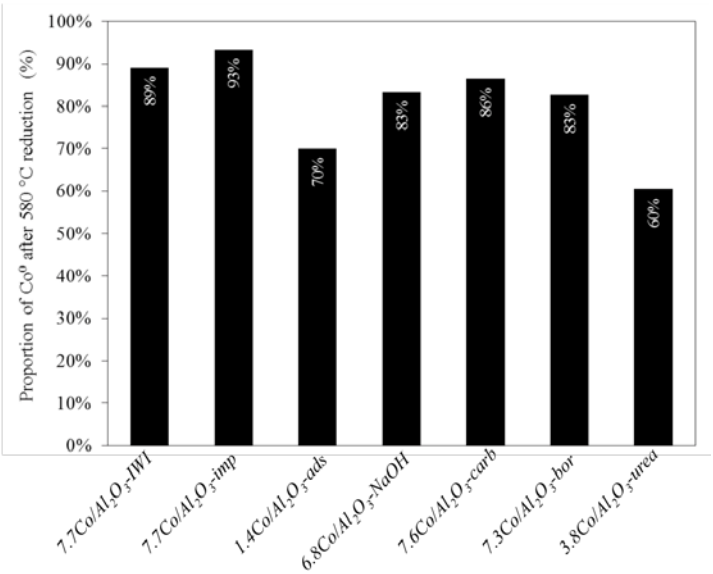

Figure 8. Proportion of Co^0 in *Co/Al_2O_3* catalysts synthesised by different methods after reduction at 580 °C determined from XPS spectra.

According to XPS derived data shown in Figure 8, the catalysts synthesised by impregnation and precipitation by NaOH, carbonate and borate buffers are the most reducible at the surface. Despite the relatively low Co surface reducibility of *3.8Co/Al_2O_3-urea* (Figure 8) estimated by XPS, the catalyst exhibited good activity which may in part be thanks to the absence of cobalt aluminate species on the TPR profile. Conversely, the low reducibility estimated by XPS of the catalyst synthesised by adsorption (*1.4Co/Al_2O_3-ads*) is reflected by the poor ammonia decomposition activity. The low reducibility of *1.4Co/Al_2O_3-ads* is in part due to the strong metal-support interaction favouring the formation of "irreducible" Co^{2+} spinel-like species ($CoAl_2O_4$), in which cobalt atoms have propagated into the γ-Al_2O_3 support lattice.

Conclusions

A range of synthetic methods including adsorption, impregnation and precipitation with a range of precipitants (urea, NaOH, borate and carbonate buffers) were used for the deposition of cobalt on an alumina support to identify the main physical properties governing the catalytic activity for hydrogen production from ammonia decomposition. Particle size plays the most important role with catalytic activity generally increasing as the cobalt particle size decreases. The catalysts prepared by precipitation with a carbonate buffer shows the highest activity within the studied range due to the small average Co^0 particle size, the high reducibility of the cobalt species and the absence of additional contaminants. Catalyst synthesis by precipitation with urea leads to the initial formation of $Co_2CO_3(OH)_2$ after calcination, rather than the typical mixed oxide Co_3O_4 obtained by the other methods, which after reduction leads to a strong-metal support interaction and consequently relatively lower reducibility of the cobalt species but nevertheless presents good activity. Conversely, precipitation with a borate buffer leaves impurities on the surface of the catalyst including potassium, boron and chlorine, which have a detrimental effect on their ammonia decomposition catalytic

activity. Impregnation methods form catalysts with highly reducible cobalt species however, weak metal-support interactions and larger particle sizes result in mediocre catalytic activities. By contrast, the use of the adsorption method produces a catalyst with a considerably lower cobalt loading due to the acidic pH during synthesis and a strong metal-support interaction, promoting the formation of inactive cobalt aluminate species, reducing the overall available Co^0. A delicate balance between small particle size and cobalt-support interaction strength to facilitate high cobalt reducibility without encouraging the formation of cobalt aluminates is identified as the key design criteria for discovery of superior cobalt-based catalysts to accelerate the rate of hydrogen release from ammonia.

Acknowledgments

The authors would like to acknowledge the UK Engineering and Physical Science Research Council (EPSRC) and Sasol UK for financial support (grant numbers EP/N013778/1 and EP/L020432/2).

References

1. Yin, S. F., Xu, B. Q., Zhou, X. P. & Au, C. T. A mini-review on ammonia decomposition catalysts for on-site generation of hydrogen for fuel cell applications. *Appl. Catal. A Gen.* **277,** 1–9 (2004).
2. Hill, A. & Torrente Murciano, L. In-situ H2 production via low temperature decomposition of ammonia : insights into the role of cesium as a promoter. *Int. J. Hydrogen Energy* **39,** 7646–7654 (2014).
3. Lan, R., Irvine, J. T. S. & Tao, S. Ammonia and related chemicals as potential indirect hydrogen storage materials. *Int. J. Hydrogen Energy* **37,** 1482–1494 (2012).
4. Klerke, A., Christensen, C. H., Nørskov, J. K. & Vegge, T. Ammonia for hydrogen storage: challenges and opportunities. *J. Mater. Chem.* **18,** 2304 (2008).
5. C. Smith, Hill, A. K. & Torrente-Murciano, L. Current and future role of Haber–Bosch ammonia in a carbon-free energy landscape. *Energy Environ. Sci.* **13,** 331–344 (2020).
6. Schüth, F., Palkovits, R., Schlögl, R. & Su, D. S. Ammonia as a possible element in an energy infrastructure: catalysts for ammonia decomposition. *Energy Environ. Sci.* **5,** 6278–6289 (2012).
7. Satyapal, S., Petrovic, J., Read, C., Thomas, G. & Ordaz, G. The U.S. Department of Energy's National Hydrogen Storage Project: Progress towards meeting hydrogen-powered vehicle requirements. *Catal. Today* **120,** 246–256 (2007).
8. Wojcik, A., Middleton, H., Damopoulos, I. & Herle, J. Van. Ammonia as a fuel in solid oxide fuel cells. *J. Power Sources* **118,** 342–348 (2003).

9. Zamfirescu, C. & Dincer, I. Ammonia as a green fuel and hydrogen source for vehicular applications. *Fuel Process. Technol.* **90,** 729–737 (2009).

10. Wang, L., Zhao, Y., Liu, C., Gong, W. & Guo, H. Plasma driven ammonia decomposition on a Fe-catalyst: eliminating surface nitrogen poisoning. *Chem. Commun.* **49,** 3787–9 (2013).

11. Hansgen, D. A., Vlachos, D. G. & Chen, J. G. Using first principles to predict bimetallic catalysts for the ammonia decomposition reaction. *Nat Chem* **2,** 484–489 (2010).

12. Jacobsen, C. *et al.* Catalyst design by interpolation in the periodic table: bimetallic ammonia synthesis catalysts. *J. Am. Chem. Soc.* **123,** 8404–8405 (2001).

13. Hill, A. K. & Torrente-Murciano, L. Low temperature H2 production from ammonia using ruthenium-based catalysts: Synergetic effect of promoter and support. *Appl. Catal. B Environ.* **172–173,** 129–135 (2015).

14. Hu, Z., Mahin, J., Datta, S., Bell, T. E. & Torrente-Murciano, L. Ru-Based Catalysts for H2 Production from Ammonia: Effect of 1D Support. *Top. Catal.* **62,** 1169–1177 (2019).

15. Hu, Z., Mahin, J. & Torrente-Murciano, L. A MOF-templated approach for designing ruthenium–cesium catalysts for hydrogen generation from ammonia. *Int. J. Hydrogen Energy* **44,** 30108–30118 (2019).

16. Mukherjee, S., Devaguptapu, S. V., Sviripa, A., Lund, C. R. F. & Wu, G. Low-temperature ammonia decomposition catalysts for hydrogen generation. *Appl. Catal. B Environ.* **226,** 162–181 (2018).

17. Lara-García, H., Mendoza-Nieto, J., Pfeiffer, H. & Torrente-Murciano, L. COx-free hydrogen production from ammonia on novel cobalt catalysts supported on 1D titanate nanotubes. *Int. J. Hydrogen Energy* **44,** 30062–30074 (2019).

18. Bell, T. E. & Torrente-Murciano, L. H2 Production via Ammonia Decomposition Using Non-Noble Metal Catalysts: A Review. *Top. Catal.* **59,** 1438–1457 (2016).

19. Wolf, A. & Schuth, F. A systematic study of the synthesis condition for the preparation of highly active gold catalysts. *Appl. Catal., A* **226,** 1–13 (2002).

20. Torrente-Murciano, L., Hill, A. K. & Bell, T. E. Ammonia decomposition over cobalt/carbon catalysts—Effect of carbon support and electron donating promoter on activity. *Catal. Today* **286,** 131–140 (2017).

21. Bell, T. E., Gonzalez-Carballo, J. M., Tooze, R. P. & Torrente-Murciano, L. Single-step synthesis of nanostructured γ-alumina with solvent reusability to maximise yield and morphological purity. *J. Mater. Chem. A* **3,** 6196–6201 (2015).

22. Xie, X. & Shen, W. Morphology control of cobalt oxide nanocrystals for promoting their catalytic performance. *Nanoscale* **1,** 50 (2009).

23. Cuenya, B. R. & Behafarid, F. Nanocatalysis: size-and shape-dependent chemisorption and catalytic reactivity. *Surf. Sci. Rep.* **70,** 135–187 (2015).

24. Haruta, M. Low-Temperature Oxidation of CO over Gold Supported on TiO2, α-Fe2O3, and Co3O4. *J. Catal.* **144,** 175–192 (1993).

25. Bezemer, G. L. *et al.* Cobalt Particle Size Effects in the Fischer−Tropsch Reaction Studied with Carbon Nanofiber Supported Catalysts. *J. Am. Chem. Soc. Soc.* **128,** 3956–3964 (2006).

26. Moodley, D. J. *et al.* The impact of cobalt aluminate formation on the deactivation of cobalt-based Fischer–Tropsch synthesis catalysts. *Catal. Today* **171,** 192–200 (2011).

27. Bolt, P. H., Habraken, F. H. P. M. & Geus, J. W. Formation of Nickel, Cobalt, Copper, and

Iron Aluminates from a- and g-Alumina-Supported Oxides: A Comparative Study. *J. Solid State Chem.* **135,** 59–69 (1998).

28. Zhang, H., Alhamed, Y. & Chu, W. Controlling Co-support interaction in Co/MWCNTs catalysts and catalytic performance for hydrogen production via NH3 decomposition. *Appl. Catal. A Gen.* **464–465,** 156–164 (2013).

29. Satterfield, C. N. *Heterogeneous catalysis in practice*. (McGraw-Hill, 1980).

30. JCPDS Associateship. New X-Ray Powder Diffraction Patterns from the JCPDS Associateship. *Powder Diffr.* **1,** 77–99 (1986).

31. Torrente-Murciano, L., He, Q., Hutchings, G. J., Kiely, C. J. & Chadwick, D. Enhanced Au-Pd Activity in the Direct Synthesis of Hydrogen Peroxide using Nanostructured Titanate Nanotube Supports. *ChemCatChem* **6,** 2531–2534 (2014).

32. Kasprzyk-Hordern, B. Chemistry of alumina, reactions in aqueous solution and its application in water treatment. *Adv. Colloid Interfac.* **110,** 19–48 (2004).

33. Jacobs, G. *et al.* Fischer–Tropsch synthesis: Temperature programmed EXAFS/XANES investigation of the influence of support type, cobalt loading, and noble metal promoter addition to the reduction behavior of cobalt oxide particles. *Appl. Catal. A Gen.* **333,** 177–191 (2007).

34. Biesinger, M. C. *et al.* Resolving surface chemical states in XPS analysis of first row transition metals, oxides and hydroxides: Cr, Mn, Fe, Co and Ni. *Appl. Surf. Sci.* **257,** 2717–2730 (2011).

35. Donaldson, J. D., Beyersmann, D., Donaldson, J. D. & Beyersmann, D. in *Ullmann's Encyclopedia of Industrial Chemistry* (Wiley-VCH Verlag GmbH & Co. KGaA, 2005). doi:10.1002/14356007.a07_281.pub2

36. Yang, J., Cheng, H. & Frost, R. L. Synthesis and characterisation of cobalt hydroxy carbonate Co2CO3(OH)2 nanomaterials. *Spectrochim. Acta Part A Mol. Biomol. Spectrosc.* **78,** 420–428 (2011).

37. Lendzion-Bielun, Z., Narkiewicz, U. & Arabczyk, W. Cobalt-based Catalysts for Ammonia Decomposition. *Materials (Basel).* **6,** 2400–2409 (2013).

38. Beer, M. de, Kunene, A., Nabaho, D., Claeys, M. & Steen, E. van. Technical and economic aspects of promotion of cobalt-based Fischer-Tropsch catalysts by noble metals–a review. *J. South. African Inst. Min. Metall.* **114,** 157–165 (2014).

39. Wu, R.-J., Wu, J.-G., Tsai, T.-K. & Yeh, C.-T. Use of cobalt oxide CoOOH in a carbon monoxide sensor operating at low temperatures. *Sensors Actuators B Chem.* **120,** 104–109 (2006).

40. James, O. O. & Maity, S. Temperature programme reduction (TPR) studies of cobalt phases in γ-alumina supported cobalt catalysts. *J. Pet. Technol. Altern. Fuels* **7,** 1–12 (2016).

41. Gu, Y.-Q. *et al.* Transition metal nanoparticles dispersed in an alumina matrix as active and stable catalysts for CO x -free hydrogen production from ammonia. *J. Mater. Chem. A* **3,** 17172–17180 (2015).

42. Bowker, M., Nuhu, A. & Soares, J. High activity supported gold catalysts by incipient wetness impregnation. *Catal. Today* **122,** 245–247 (2007).

43. Tsakoumis, N. E., Rønning, M., Borg, Ø., Rytter, E. & Holmen, A. Deactivation of cobalt based Fischer–Tropsch catalysts: A review. *Catal. Today* **154,** 162–182 (2010).